Journal of Cell Science 110, 975-983 (1997)
Printed in Great Britain © The Company of Biologists Limited 1997
JCS4342

Imaging of Ca^{2+} transients induced in *Paramecium* cells by a polyamine secretagogue

Norbert Klauke and Helmut Plattner*

Faculty of Biology, University of Konstanz, PO Box 5560, D-78434 Konstanz, Germany

*Author for correspondence

SUMMARY

In *Paramecium tetraurelia* cells analysis of transient changes in Ca^{2+} concentration, $[Ca^{2+}]_i$, during aminoethyldextran (AED) stimulated synchronous (<1 second) trichocyst exocytosis has been hampered by various technical problems which we now have overcome. While Fura Red was found appropriate for quantitative double wavelength recordings, Fluo-3 allowed to follow, semi-quantitatively but with high time resolution, $[Ca^{2+}]_i$ changes by rapid confocal laser scanning microscopy (CLSM). Resting values are between 50 and 70 nM in the strains analysed (7S wild type, as well as a non-discharge and a trichocyst-free mutant, nd9-28°C and tl). In all strains $[Ca^{2+}]_i$ first increases at the site of AED application, up to 10-fold above basal values, followed by a spillover into deeper cell regions. This might: (i) allow a vigorous Ca^{2+} flush during activation, and subsequently (ii) facilitate re-establishment of Ca^{2+} homeostasis within ≥20 seconds. Because of cell dislocation during vigorous trichocyst exocytosis, 7S cells could be reasonably analysed only by CLSM after Fluo-3 injection. In 7S cells cortical $[Ca^{2+}]_i$ transients are strictly parallelled by trichocyst exocytosis, i.e. in the subsecond time range and precisely at the site of AED application. Injection of Ca^{2+} is a much less efficient trigger for exocytosis. Ca^{2+}-buffer injections suggest a requirement of $[Ca^{2+}]_i$ >1 to 10 μM for exocytosis to occur in response to AED. In conclusion, our data indicate: (i) correlation of cortical $[Ca^{2+}]_i$ transients with exocytosis, as well as (ii) occurrence of a similar signal transduction mechanism in mutant cells where target structures may be defective or absent.

Key words: Calcium, Exocytosis, *Paramecium*, Secretion

INTRODUCTION

Since the development of Ca^{2+}-sensitive fluorochromes (Tsien, 1988) it has been documented with many cells that a transient increase in free Ca^{2+} concentration, $[Ca^{2+}]_i$, in the cell cortex accompanies stimulated exocytosis. Ca^{2+} may, thus, be an important regulator of exocytosis (Tsien and Tsien, 1990; Burgoyne and Morgan, 1993; Cheek and Barry, 1993; Bootman and Berridge, 1995; Clapham, 1995).

Although the *Paramecium* cell is an established model system to analyse several aspects of triggered exocytosis (Plattner et al., 1991), also with the implication of Ca^{2+} as a regulator, $[Ca^{2+}]_i$ transients have not been documented so far because of a variety of severe technical problems. (i) As a ciliated protozoan this cell is highly mobile. (ii) During vigorous trichocyst discharge cells can be locally deformed and displaced. (iii) They do not readily take up fluorochrome esters. (iv) Once incorporated, fluorochromes may be sequestered into digesting vacuoles.

We now have immobilized cells for microinjection with different fluorochromes, not only for conventional but also for confocal laser scanning microscopy (CLSM) with high time resolution. For the technical reasons mentioned we have included non-secretory strains in our analyses. Thus, we can show for the first time calibrated resting values, $[Ca^{2+}]_i^{rest}$, and rapid local transients during activation, $[Ca^{2+}]_i^{act}$, by the secretagogue aminoethyldextran (AED). Within the cell cortex, $[Ca^{2+}]_i^{act}$ may culminate very rapidly after stimulation, i.e. at ≤2 seconds by conventional analyses and even much faster according to CLSM. Then rapid spillover into deeper cell layers occurs, followed by slow recovery. In wild-type cells a cortical $[Ca^{2+}]_i^{act}$ transient rise to >1 to 10 μM is accompanied by fast synchronous trichocyst exocytosis. Experiments with some exocytosis-incompetent mutants show similar Ca^{2+} signals. Microinjected chelators of different Ca^{2+}-affinity indicate that $[Ca^{2+}]_i$ may have to rise locally well beyond 1 μM for exocytosis to occur.

MATERIALS AND METHODS

Cell cultures

Cultures of *Paramecium tetraurelia*, wild-type (strain 7S) and trichocyst-free mutant cells (trichless, tl; Pollack, 1974) were grown at 25°C; strain nd9 with docked but non-dischargeable trichocysts (Beisson et al., 1976) was grown at non-permissive 28°C, all in dried lettuce medium monoxenically inoculated with *Enterobacter aerogenes* containing $[Ca^{2+}] = 0.5 \times 10^{-4}$ M. Mutants were grown to early stationary phase, 7S cells to mid-logarithmic phase and concentrated before use to 10^5 cells/ml by low-speed centrifugation.

Microinjections and trigger experiments

Individual cells were transferred under a dissecting microscope into 1 µl droplets of culture medium on a siliconized glass slide and covered with paraffin oil to prevent evaporation. In an inverted microscope (ICM 405, Zeiss, Oberkochen, Germany) a sucking capillary of ~10 µm inner diameter was used to aspirate excess fluid and, thus, to immobilize isolated cells for microinjection. Ca^{2+}-sensitive fluor-ochromes, dissolved in 10 mM Tris-HCl, pH 7.2, were microinjected as indicated by Kersken et al. (1986), to yield a final concentration of 50 (Fura Red) to 100 µM (Fura-2, Fluo-3). The volume injected was ~10^{-11} l, i.e. ~10% of cell volume. All intracellular concentrations indicated are estimated final concentrations. In controls, equal distribution throughout the cell body was ascertained, e.g. after 0.5 to 2 minutes, by confocal laser scanning microscopy, CLSM, as described below. A solution of 1% AED was pressure ejected (0.1 seconds) from a second capillary and the dilution factor, yielding a EC_{100} = 0.05% (Plattner et al., 1984, 1985), was estimated by free fluorescein added. Usually final $[Ca^{2+}]_e$ was 50 µM in trigger experiments.

$[Ca^{2+}]_i$ increase during AED stimulation was eventually manipulated by injection of BAPTA or 4,4′-difluoro-BAPTA (Molecular Probes, Eugene, OR). Alternatively, we have injected $CaCl_2$ after loading cells with Fura Red (for details, see Results).

Fluorometry, calibrations and image analysis

Fluorochromes used, Fura-2, Fura Red and Fluo-3, were all from Molecular Probes and were all microinjected.

Fura-2 and Fura Red were detected in the ICM 405 microscope (Zeiss) as follows. Excitation light was selected from a 50 W mercury lamp (HBO 50, Osram) by a 10 nm bandpass interference filter (360 and 380 nm for Fura-2, 440 and 490 nm for Fura Red; from L.O.T., Darmstadt, Germany) mounted on a home-made filter wheel (mechanically separated from the microscope) and reflected into the objective (63/1.3 oil, Zeiss) using a dichroic mirror (FT 460 for Fura-2, FT 510 nm for Fura Red, Zeiss). Emission was collected by the objective and passed the dichroic and barrier filter (LP 470 nm for Fura-2, LP 590 nm for Fura Red, Zeiss) before reaching the image intensifier of a moonlight camera from Panasonic (AVT Horn, Aalen, Germany). Diffusion of Fura Red into outermost cell layers was analysed by z-series in a CLSM operated at 488 nm excitation (50 mW Ar-laser output) and a longpass filter of 510 nm.

Fluorescence was excited for 250 milliseconds at each wavelength and, during turning of the filter wheel, phase contrast images were eventually taken to control cell behaviour. One cycle consisting of two fluorescence and one phase contrast image, thus, lasted 2 seconds.

Conventional fluorescence images were digitized on a 486 PC equipped with a framegrabber and ratio-imaging was performed with Image-1 software (Universal Image Cooperation, West-Chester, PA, USA) resulting in a false-colour picture of the cell. Alternatively average fluorescence intensities were measured at both excitation wavelengths and for each situation the ratio was calculated (Sigma Plot, Jandel Scientific Software, Corte Madera, CA, USA) and converted to $[Ca^{2+}]$ according to calibration curves for $[Ca^{2+}]$. These were obtained by adding different amounts of $CaCl_2$ to a solution containing 10 mM Na_2Pipes, 50 mM KCl, 5 mM NaCl and 10 mM EGTA, pH 7.0. $[Ca^{2+}]$ was calculated using a software program (Föhr et al., 1993) for conditions closely resembling ionic conditions in *Paramecium* cells (Lumpert et al., 1990; see Results). To mimic optical path conditions, calibration solutions with fluorochromes were filled in rectangular microcapillaries of 50 µm lumen (thickness of a *Paramecium* cell) for $[Ca^{2+}]$ calibration in the fluorescence microscope.

Semi-quantitative Ca^{2+} measurements were done with a confocal laser scanning system (Odyssey, Noran Instruments, Middleton, WI, and Bruchsal, Germany), with 33 frames/second acquisition rate by optoacustic beam deflection. This was mounted on an inverted microscope (Axiovert form Zeiss) equipped with an oil immersion objective (63/1.4, Zeiss). In Fluo-3 injected cells a rise of $[Ca^{2+}]$ was shown by an increase in fluorescence intensity at ≥514 nm referred to the fluorescence before stimulation (f/f_o), with excitation at 488 nm, as used in other CLSM studies (Bacskai et al., 1995). In some experiments alternate acquisition of fluorescence images and images generated by the laser light passing the cell was used to correlate Ca^{2+} signals with exocytosis.

RESULTS

Methodical aspects

Attempts to incubate cell suspensions with fluorochrome esters were unsuccessful because of lack of uptake. Injection of fluorochrome salt into immobilized cells was achieved by isolation in a small droplet and cautious reduction of the volume, to mechanically stop swimming activity, as described in Materials and Methods. Such cells could be locally triggered with AED through a closely apposed capillary by pressure ejection and superfusion. When mimicked by buffer application only these procedures did not cause any important changes in global $[Ca^{2+}]_i$ (Table 1-B) with different fluorochromes.

Because of lack of any information with our system and since we had to compare conventional double wavelength with single wavelength CLSM recording, we had to try out different fluorochromes. Calibration of Fura Red revealed suitability for our cells in a linear range between ≥20 nM and ≤5 µM, i.e. close to the manufacturer's specifications, and a similar curve was obtained for Fura-2 (not shown). For CLSM analysis a fluorochrome with lower Ca^{2+} affinity was advised since within short periods relatively high $[Ca^{2+}]_i^{act}$ had to be expected. Fluo-3 is reported as suitable for 30 nM-4 µM (Minta et al., 1989).

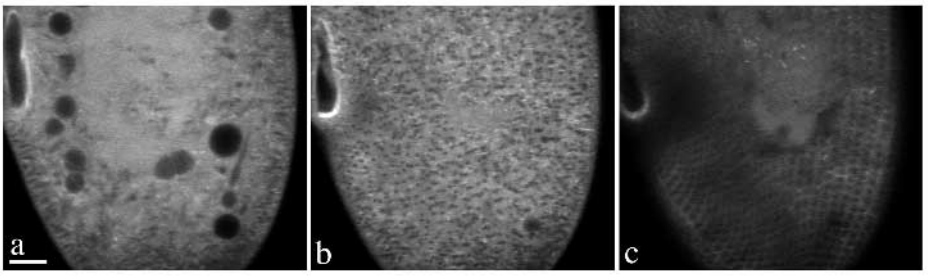

Fig. 1. Even distribution of Fura Red (50 µM) 2 minutes after injection. Documentation in a CLSM by 488 nm excitation and 514 nm emission in a nd9-28°C cell in (a) median, (b) cortical and (c) superficial cell layers. Note exclusion of fluorochrome from vacuoles, including a pulsatile vacuole at the lower right in a, and from the numerous docked trichocysts in a and b, while c shows penetration of Fura Red into the outermost cell surface layers. Bar, 10 µm.

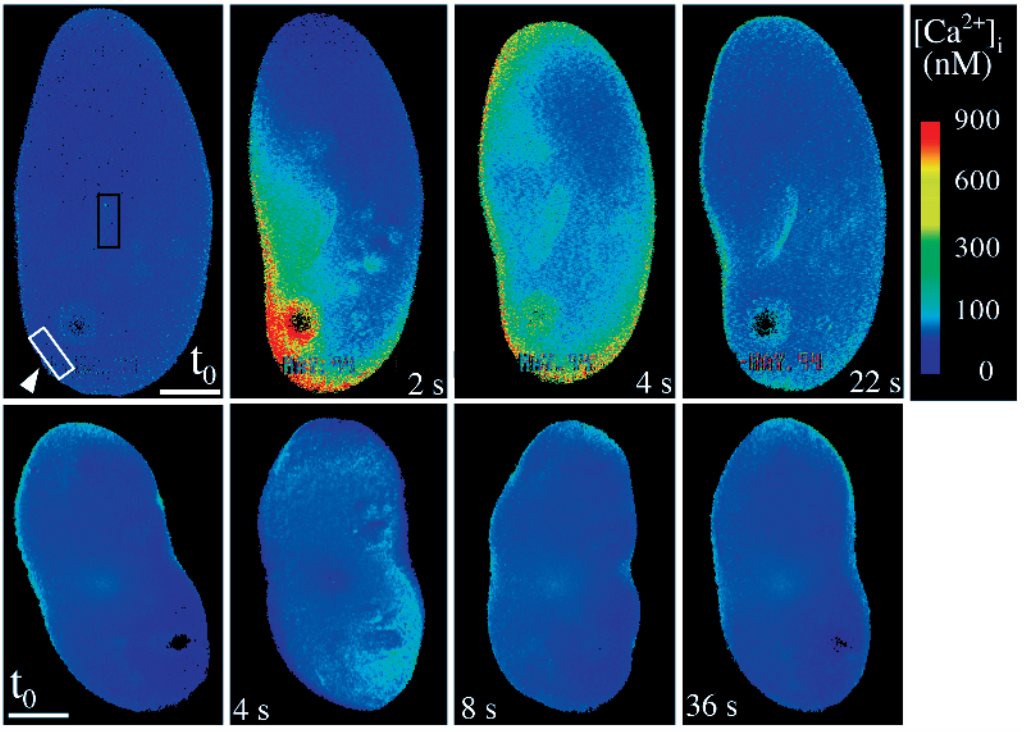

Fig. 2. Visualization of $[Ca^{2+}]_i$ change in a Fura Red (50 μM) loaded nd9-28°C cell in response to AED (top) and absence of response after mock stimulation (bottom). Top: false colour images show the cell at rest (t_o) and at times indicated after stimulation by AED (0.05% estimated concentration at cell surface) applied at arrowhead. Note that $[Ca^{2+}]_i$ first rises, within 2 seconds, at the cortical area where superfusion with AED begins. Within 4 seconds the signal sweeps deeper inside the cell and within 22 seconds the Ca^{2+} response decays to resting level. During diastole the posterior contractile vacuole is visible as a black hole. Framed areas are for quantitation of cortical or central $[Ca^{2+}]_i$ changes, respectively, in Fig. 4. Bottom: in controls (buffer application), no change in $[Ca^{2+}]_i$ is recognized. Bars, 20 μm.

K_d values under ionic conditions closely resembling our cells (Lumpert et al., 1990) are 130 nM for Fura Red (manufacturer's data), 170 nM for Fura-2 (Pethig et al., 1989) and 400 nM for Fluo-3 (Minta et al., 1989). An important prerequisite is even distribution of fluorochromes throughout the interior of the cells, up to the outermost layers. This is shown specifically for Fura Red by CLSM single wavelength recording (Fig. 1). While most fluorochromes used are excluded from pulsatile and digesting vacuoles as well as from trichocysts (Fig. 1), this is not true for Fluo-3 (see below). Sequestration into some of the digesting vacuoles is finished within ~1 minute after injection and does not change subsequently, i.e. when $[Ca^{2+}]_i$ analysis is performed.

Fura-2 registrations showed $[Ca^{2+}]_i^{rest}$ = 80 nM in 7S cells, but Fura-2 proved problematic because of notorious photoactivation (Grapengiesser, 1993) resulting in exocytosis at a global threshold of $[Ca^{2+}]_i \geq 400$ nM (not shown). We then tested Fura Red and Fluo-3 for suitability. In the three strains analysed $[Ca^{2+}]_i^{rest}$ remains rather constant around 50 nM over 20 seconds (Table 1-A), i.e. the usual $[Ca^{2+}]$ transient recording time, and even beyond 1 minute. This largely excludes cell impairment. Using Fluo-3 with CLSM in 7S cells, only a small fluorescence change was observed during continuous laser illumination over 20 seconds (Table 1-A) or more.

Table 1. Constancy of global $[Ca^{2+}]_i^{rest}$ in different strains

	$[Ca^{2+}]_i^{rest}$, (nM)		
Strain/time	t_o	4 seconds	20 seconds
(A)			
7S	59	61	66
nd9-28°C	36	43	45
tl	66	71	66
7S (f/f_o)	1.00	1.15	1.24
(B)			
nd9-28°C (*n*=5)	48±10	53±10	66±15
tl (*n*=3)	65±10	63±10	75±20

Fluorochrome analysis started at t_o (A) without and (B) during a flush with buffer (0.1 second, also starting at t_o, without secretagogue added). Values were determined with Fura Red (50 μM), except for f/f_o ratios (determined with 100 μM Fluo-3 to control absence of photosensitization during confocal analysis). Values in A are typical for a total of 5 cells analysed in each case (for mean values, see Table 2). ± values indicate standard errors.

Conventional double wavelength recordings

Mechanical restraints were required for analysing 7S cells since they move quickly particularly during exocytosis (see Introduction). Therefore, we started with mutants for controls. Both, nd9-28°C and tl cells show rapid $[Ca^{2+}]_i$ increase at the site of AED application (Figs 2 and 3 top). As AED spreads around a cell, a cortical $[Ca^{2+}]_i$ transient also spreads over increasing cell surface areas. Simultaneously Ca^{2+} sweeps the cell interior. In the examples shown $[Ca^{2+}]_i^{rest}$ may be re-established within a short time, but this may mostly last ≥20 seconds. Mock stimulation by buffer application causes no remarkable $[Ca^{2+}]_i$ change (Figs 2 and 3 bottom; Table 1-B).

$[Ca^{2+}]_i$ transients are evaluated quantitatively in Fig. 4 for nd9-28°C and in Fig. 5 for tl cells, respectively. Analysis of global changes (Table 2) blurrs actual dynamics, although it facilitates estimation of the total Ca^{2+} load in cells during stimulation (see Discussion). Whereas global values culminate at 4 seconds, about 3 to 5 times the basal $[Ca^{2+}]_i$ values, spatially resolved evaluation shows that $[Ca^{2+}]_i^{act}$ peaks already 2 seconds after AED application in nd9-28°C cells (Fig. 4). This is at the time resolution limited by filter change. Surprisingly data obtained with tl cells are much more variable (Fig. 5).

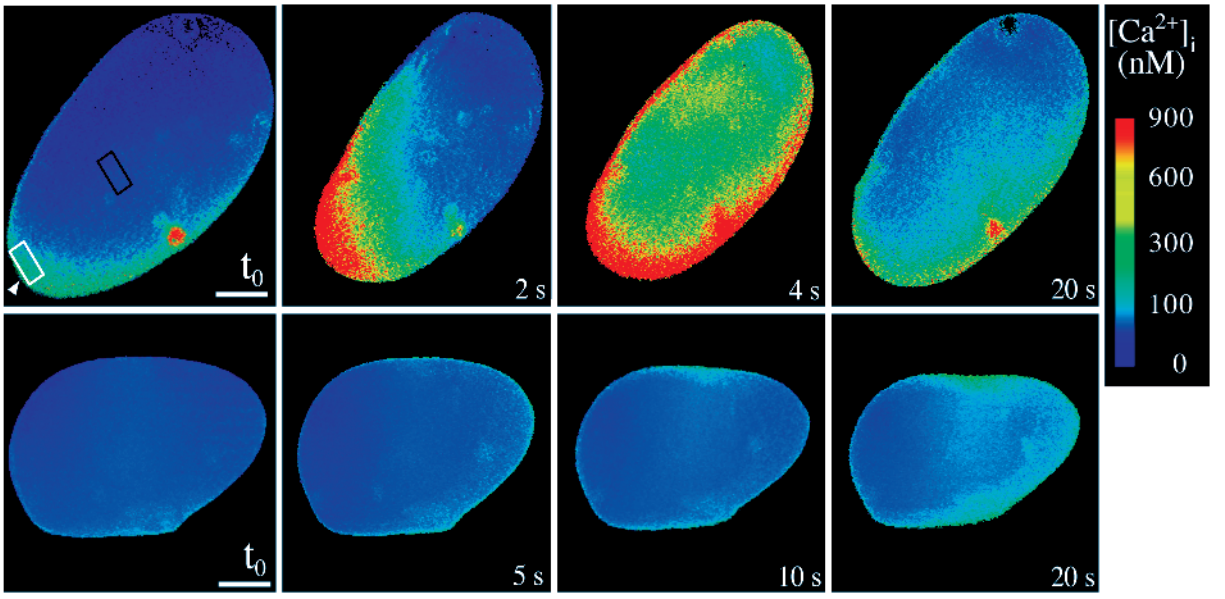

Fig. 3. Visualization of $[Ca^{2+}]_i$ change in a Fura Red (50 µM) loaded tl cell, (top) in response to AED (applied at arrowhead) or (bottom) after mock stimulation (buffer only). Note in the top row signal spread first along the cell surface and then into central regions, followed by recovery within 20 seconds. In the bottom row $[Ca^{2+}]_i$ remains unchanged. Boxed areas are evaluated in Fig. 5 (bottom). Bars, 20 µm.

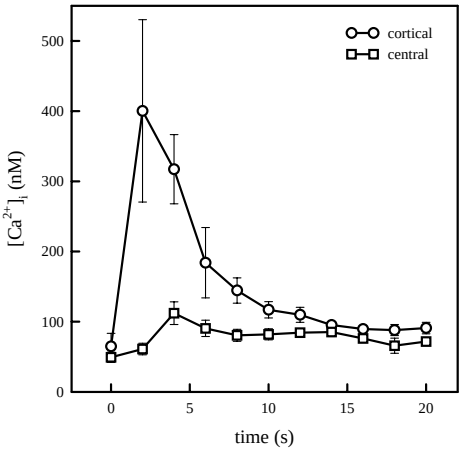

Fig. 4. Time course of spatially resolved $[Ca^{2+}]_i$ changes in cortical and central regions of Fura Red injected nd9-28°C cells following AED stimulation under conditions indicated in Fig. 2 (boxed areas). Note centropetal signal spread. Stimulated values decline to resting level within ~15 seconds. Bars indicate standard errors, *n*=5.

With both strains analysed, more or less pronounced Ca^{2+} transients reach deeper cell regions and $[Ca^{2+}]_i^{rest}$ may not yet be fully re-established after 20 seconds (Table 2). Time required for filter change did not allow similar analyses with fast moving 7S cells.

CLSM analysis with improved time resolution

Therefore, we switched to high time resolution, using Fluo-3 injection in conjunction with CLSM. First we analysed nd9-28°C cells for comparison with previous double wavelength recordings and then Fluo-3 loaded 7S cells to visualize Ca^{2+} transients in spite of cell displacement and deformation during trichocyst discharge (see Introduction). Semi-quantitative evaluation of signals was by the ratio f/f_o, i.e. fluorescence after stimulation vs values at rest, when images were taken in minimal intervals of 33 milliseconds (see Materials and Methods).

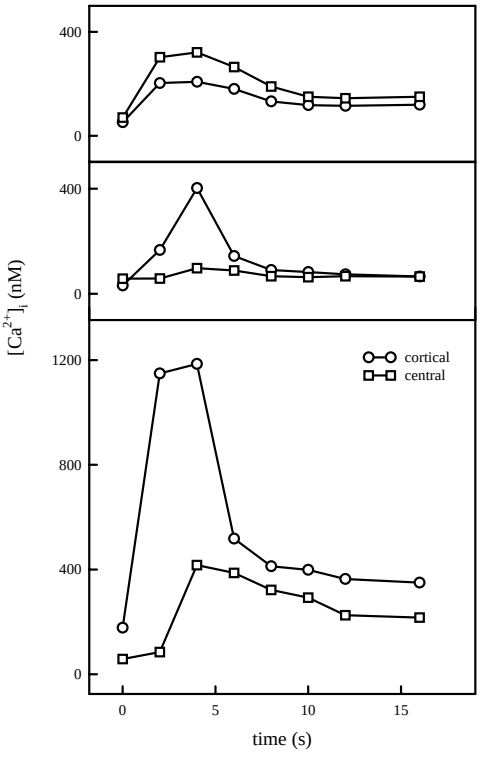

Fig. 5. $[Ca^{2+}]_i$ changes in cortical and central areas of three Fura Red injected tl cells after AED stimulation under conditions specified in Fig. 4. Note wide variation between individual cells.

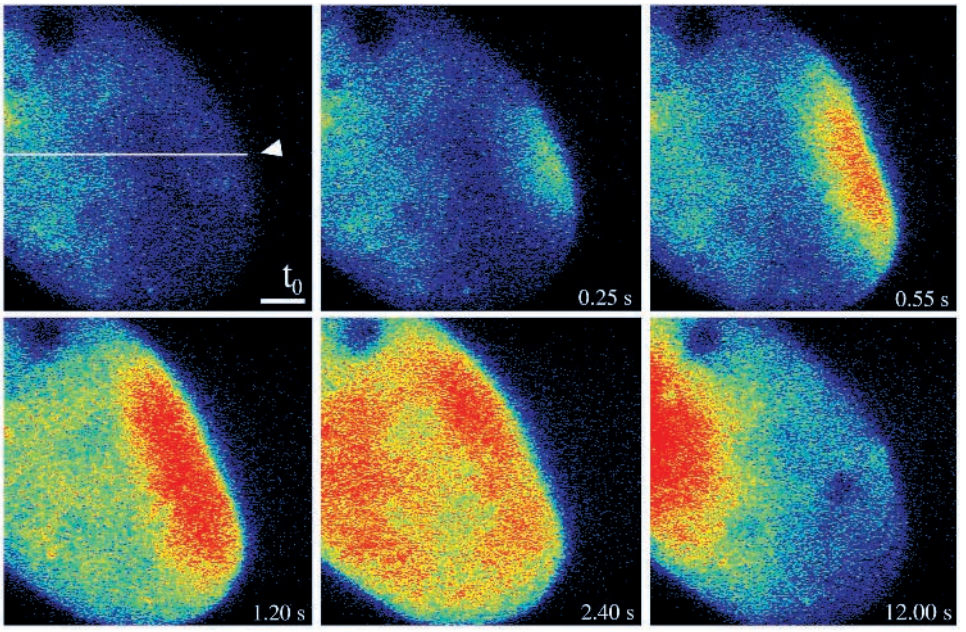

Fig. 6. AED induced signal in a Fluo-3 (100 μM) injected nd9-28°C cell evaluated by CLSM. Top: false colour images show a typical example of locally variable fluorescence brightness at rest (t_o) and increase at times indicated after AED stimulation (arrowhead). Bar, 10 μm. Changes in Fluo-3 brightness with time were measured with all pictures available (8 images/second) along a 60 μm long line from the cell boundary to the interior as indicated in the first picture (t_o). Bottom: 3-D plot of line scans at different times after AED application as shown in the false colour images above. Note spillover of Ca^{2+} from the cell cortex to the interior of the cell. Pictures were filtered to reduce the noise during scanning of fluorescence signals.

Table 2. Global $[Ca^{2+}]_i^{rest}$ and its change in different strains after AED stimulation

	$[Ca^{2+}]_i$, (nM)		
Strain	Global rest (t_o)	Global maximum (2 to 4 seconds)	Global recovery (20 seconds)
7S (*n*=12)	68±5	nd*	nd*
nd9-28°C (*n*=5)	48±10	133±25	82±10
tl (*n*=3)	48±5	250±40	73±5

Cells injected with Fura Red (50 μM) followed by double wavelength evaluation. ± standard errors.

*nd = not done with the method indicated above because of cell deformation and displacement during trichocyst discharge. For estimations in 7S cells by other methods, see text.

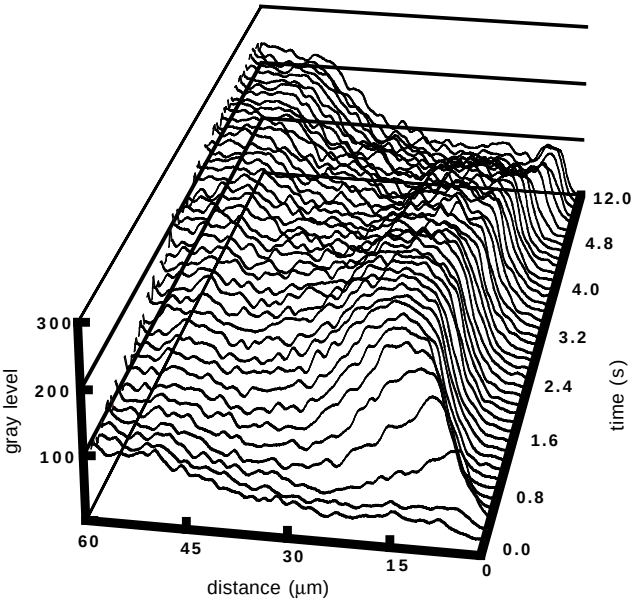

Fig. 6 shows $[Ca^{2+}]_i$ increase in a nd9-28°C cell, again starting from the site of AED application, from where the signal spreads laterally and inside the cell. Cortical signal increases within 1 second to about 9 times basal values. We attribute this faster increase, though to relative values approaching those reported in Fig. 4, to improved resolution with CLSM. Concomitantly the line scan evaluation in Fig. 6 (bottom) shows continuous spillover into deeper cell regions. From this we could expect realistic data for 7S cells.

To obtain methodically unimpaired semi-quantitative data for 7S cells we used different approaches. In a first approach we applied only a brief AED stimulus (which remained locally restricted according to extracellular emission from fluorescein added), thus reducing cell dislocation (Fig. 7). Under these conditions cortical $[Ca^{2+}]_i^{act}$ rose, though only locally, considerably above basal levels and the Ca^{2+}-signal was paralleled by local trichocyst exocytosis.

We then mimicked conditions of mutant cells by producing tl phenocopies from 7S cells. We depleted Fluo-3 loaded 7S cells of their trichocysts by an AED stimulus, before exposure to a second AED stimulus 10 minutes later. By this time interval Ca^{2+} homeostasis can be reasonably assumed to be re-established. The second stimulus also results in considerable cortical $[Ca^{2+}]_i$ increase by a factor of 3 (Figs 8 and 9). From $[Ca^{2+}]_i^{rest}$ = 68 nM determined conventionally (Table 2) one may derive a cortical peak value of $[Ca^{2+}]_i^{act}$ = 210 nM in 7S cells. (This smaller response may be due to only partial store refilling). These double trigger experiments also showed Ca^{2+} spillover into central cell regions, just as with mutants.

Ca^{2+} and Ca^{2+}-buffer injections

Can Ca^{2+} injection induce exocytosis and can exocytosis be suppressed by injected Ca^{2+} chelators? In Fig. 10 the Ca^{2+} injected would amount to 500 μM, disregarding cytosolic binding and pumping activities. Actual $[Ca^{2+}]_i$ values recorded in this typical experiment, however, are only 1.03 μM (at 2 seconds around injection needle) and 685 or 900 nM

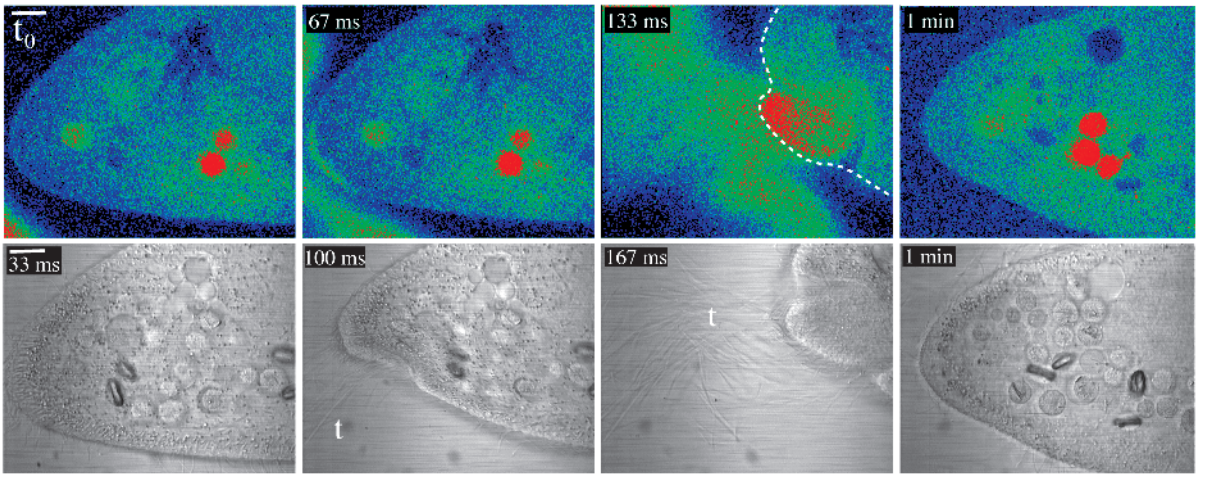

Fig. 7. Fluo-3 injected 7S cell, with AED application from a capillary at lower left. Supplementation of AED with fluorescein allows us to visualize contact of secretagogue with the cell and, by intermittent transmitted and fluorochrome images, correlation with local $[Ca^{2+}]_i$ increase and exocytosis of some trichocysts (t). Note increasing $[Ca^{2+}]_i$ within a restricted cortical zone, paralleled by local deformation (dashed line) and displacement of the cell due to ongoing release of trichocysts visible as needles outside the cell. Note that Fluo-3 exclusion from pulsatile vacuole (dark structure, top) and partial sequestration in some phagosomes (red spheres, bottom) does not change during analysis. Bar, 10 μm.

in cell cortex after 2 or 4 seconds, respectively, where it entails trichocyst exocytosis. This heavy Ca^{2+} load is only slowly down-regulated to resting level (50 nM at t_o) since global concentration is still 240 nM after 20 seconds. These experiments showed that: (i) the *Paramecium* cytoplasm has a very high Ca^{2+} buffering and/or sequestration capacity; (ii) that trichocyst release may require ≥1 μM Ca^{2+}, possibly up to 10 μM; and finally (iii) that micromolar $[Ca^{2+}]_i$ can cause local cell contraction. A similar threshold $[Ca^{2+}]_i^{act}$ value of >1 μM was estimated by the effect of AED application after injection of Ca^{2+} buffers (Table 3). While BAPTA incompletely inhibited exocytosis, the lower affinity derivative, 4,4′-F_2-BAPTA blocked exocytosis in 5 out of a total of 8 cells.

DISCUSSION

Methodical aspects

Up to now serious methodical problems have impeded imaging of $[Ca^{2+}]_i$ transients during exocytosis in *Paramecium* cells, e.g. cell movement, deformation and dislocation during trichocyst release, lack of penetration of fluorochromes, and their intracellular sequestration. We now have largely overcome these problems, however, some blurring of cortical $[Ca^{2+}]$ still may impair our measurements, even with fast CLSM. As a semi-quantitative method this also required, in parallel, quantitative double wavelength measurements to make data more reliable. During AED application this could be achieved best with exocytosis incompetent strains.

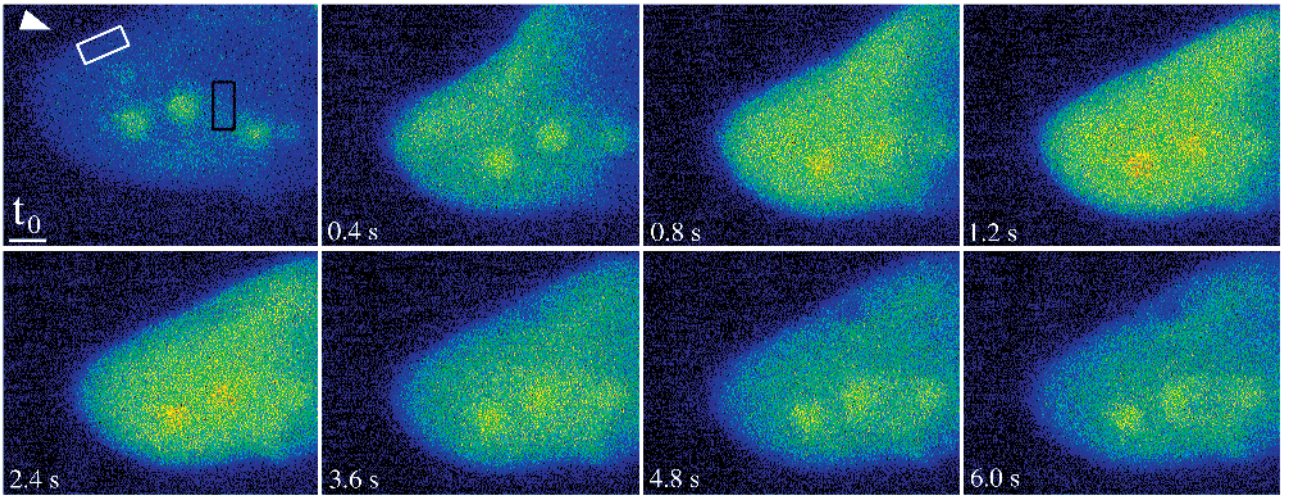

Fig. 8. Fluo-3 loaded 7S cell after double AED triggering in a 10 minute interval. This facilitates CLSM analysis due to the reduction of cell movement and/or shape change in response to the second AED application (arrowhead) after trichocyst depletion. Note equal signal spread throughout cell, aside from some Fluo-3 sequestration in large food vacuoles. Boxed areas are examples of quantitations shown in Fig. 9. Bar, 10 μm.

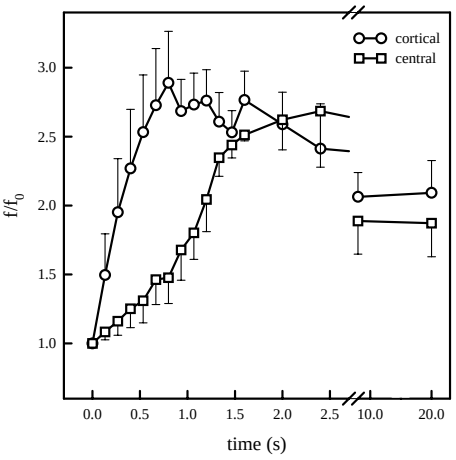

Fig. 9. Time course of f/f_0 Fluo-3 signal in 7S cells, cortical and central regions, in response to AED, as specified in Fig. 8. Bars indicate standard errors, *n*=5.

Table 3. Injected Ca^{2+}-chelators inhibit exocytosis, while injected Ca^{2+} causes little local exocytosis*

Injected compound†	K_d‡ [μM]	*n*§	Trigger¶	Exocytotic response**
Tris-HCl	–	9	–	–
	–	9	AED	+++
$CaCl_2$, 500 μM		8	–	+ (local)
BAPTA, 1 mM	0.21	10	AED	+
4,4′-F_2-BAPTA, 1 mM	1.7	5	AED	–
		3	AED	+

*7S cells, $[Ca^{2+}]_e$ = 50 μM.

†Compounds dissolved in Tris-HCl, 1 mM, pH 7.2. Intracellular concentrations estimated after injection.

‡Values indicated by Pethig et al. (1989) for an ionic strength equivalent of 100 mM KCl.

§*n*=number of cells analysed.

¶Exogenous application of 0.01% AED, e.g. 2 minutes after chelator injection.

**Trichocyst exocytosis monitored with phase contrast optics, classified as follows: –= no exocytosis, + = 1/3, ++ = 1/3 to 2/3, +++ = 3/3, i.e. all of the available trichocysts are released.

Fluorochromes were found to rapidly distribute all over the cell, although we can neither establish their availability in the narrow subplasmalemmal space nor can we record signals selectively from this critical region. Measurements with Fura-2 support values for $[Ca^{2+}]_i^{rest}$ obtained with Fura Red, but it caused photoactivation and exocytosis at $[Ca^{2+}]_i$ ≥400 nM. After AED-stimulation similar activation values were measured with Fura Red (see Results). Hence, Fura-2 had to be abandoned. Fluo-3 was most appropriate for CLSM, but it was partially sequestered into vacuoles. Since trapping occurred before activation analyses, it should not have affected our recordings.

As discussed below, the data we obtained for Ca^{2+}-signalling during secretagogue application are well comparable with other systems (for review, see Bootman and Berridge, 1995).

Biological aspects

Ironically *Paramecium* was among the first cells whose Ca channels could be well defined by electrophysiology (voltage-dependent channels in ciliary membranes; Eckert and Brehm, 1979), while Ca^{2+} imaging had to wait up to now. Still we do not yet know the molecular identity of Ca channels involved in exocytosis. Yet we can exclude ciliary Ca channels (Plattner et al., 1984) and, thus, conclude that any Ca^{2+} influx, in parallel to store activation, takes place along the somatic cell membrane (Erxleben and Plattner, 1994).

Estimations of $[Ca^{2+}]_i^{rest}$ in *Paramecium* by electrophysiology (Naitoh and Kaneko, 1972; Nakaoka et al., 1984; Machemer, 1989) are slightly above our values. This explains the occurrence of a Ca^{2+} influx even at $[Ca^{2+}]_e$ = 40 μM in

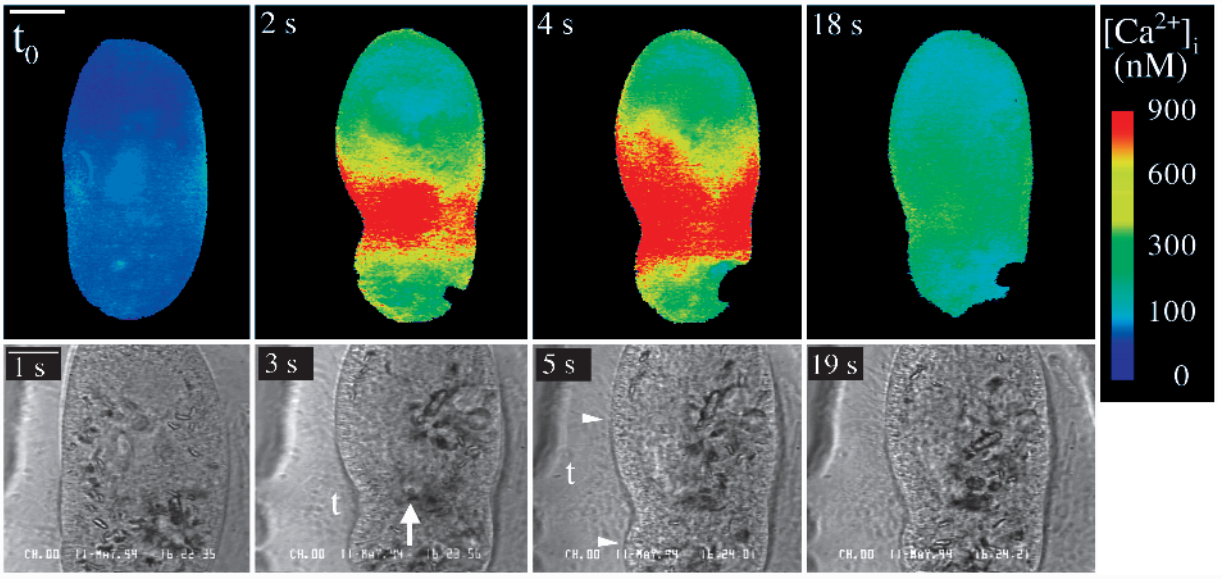

Fig. 10. This 7S cell, loaded with 50 μM Fura Red, was injected via a capillary (at arrow) with nominally 500 μM Ca^{2+} (referred to cell volume assuming equal distribution). $[Ca^{2+}]$ raised locally to ≥1 μM within 2 seconds, also in the cell cortex. The region of high $[Ca^{2+}]$ spread only to a limited extent and never reached the cell poles. Values returned to almost basal levels within >18 seconds. Note that exocytosis of trichocysts (t) remains very restricted, even in regions with high cortical $[Ca^{2+}]$ (within arrowheads) where many docked trichocysts are retained. Bar, 20 μm.

response to AED (Kerboeuf and Cohen, 1990), i.e. close to the conditions we normally work with (50 μM). We now show a rapid increase in cortical $[Ca^{2+}]_i$, in parallel to AED stimulated trichocyst exocytosis, though the time correlation we can achieve, even with CLSM, is just at the limits of AED induced exocytosis. According to our previous quenched-flow/ultrastructural analyses trichocyst release is completed within 80 milliseconds (Knoll et al., 1991).

As discussed below, we have to envisage two sources of Ca^{2+}: (i) influx from the medium; and (ii) mobilisation from the vast subplasmalemmal pools, i.e. the alveolar sacs (Stelly et al., 1991, 1995). How could these two components account for the Ca^{2+} transients observed?

During AED stimulation, $^{45}Ca^{2+}$ flux measurements showed uptake of 5 fMoles Ca^{2+} per cell (Knoll et al., 1992). Based on analytical microscopic methods, about half of the Ca stored in alveolar sacs, in a concentration of ~5 mM, may be mobilised during AED stimulation (Stelly et al., 1995). Ca^{2+} influx would necessarily increase cortical $[Ca^{2+}]_i$ primarily in the ~15 nm narrow subcortical space between cell membrane and alveolar sacs (Plattner et al., 1991). According to morphometric evaluations this subplasmalemmal space has a volume of 160 μm^3 (Erxleben et al., 1997). Possibly Ca^{2+} released from alveolar sacs could also flow selectively into this space. If one would disregard Ca^{2+} diffusion and binding, as well as sequestration and extrusion, Ca^{2+} influx and mobilisation would result in concentrations in the subplasmalemmal compartment ~10^5 times above measured values (Erxleben et al., 1997, and this paper), thus by far reversing gradients. This is rapidly counteracted and requires further explanation. $[Ca^{2+}]$ transients might be too rapid to be detected even by fast CLSM with a 'fast' fluorochrome. Although time points achieved with Fluo-3/CLSM are within the range of synchrony of AED induced exocytosis (Knoll et al., 1991), signal build cannot compete with recordings of Ca^{2+}-activated currents which accompany individual AED stimulated exocytotic events (Erxleben and Plattner, 1994), with a rise time of 7 milliseconds and a half width of 21 milliseconds (Erxleben et al., 1997). As found with motor nerve endings by electrophysiology actual $[Ca^{2+}]_i^{act}$ values precisely at exocytosis sites may be as high as several 100 μM for milliseconds (Llinás et al., 1995; Zucker, 1993). Although similar values would appear possible (see above), fluorescence data obtained with our system show a greater resemblance to chromaffin cells with ≤10 μM $[Ca^{2+}]_i^{act}$ within 30 milliseconds (Chow et al., 1994), Purkinje cells with ≤3 μM within 100 milliseconds (Eilers et al., 1995) or cerebellar granule cells with several 100 nM $[Ca^{2+}]_i^{act}$ during a similar time range (Regehr and Atluri, 1995). Additionally any build-up of subplasmalemmal $[Ca^{2+}]$ may be quickly counterregulated by the mechanisms mentioned and, thus, restrict the lifetime of current signals. With this regard the spillover into the cell body which we observe may be of particular functional interest (see below).

All these restrictions in interpreting actual $[Ca^{2+}]_i^{act}$ values at exocytosis sites, however, concern any Ca^{2+} imaging study (Morgan, 1993; Ross, 1993) and, to some extent, even electrophysiological measurements (Augustine and Neher, 1992; Bootman and Berridge, 1995).

To compensate for these problems one can inject Ca^{2+} buffers of different sensitivities and kinetics before stimulation. For instance, BAPTA has a lower K_d than its low affinity difluoro-derivative (Table 3). Due to very rapid Ca^{2+} binding kinetics this allows us to estimate local $[Ca^{2+}]_i^{act}$ well within <1 milliseconds in a region <1 μm around a Ca^{2+} source, as calculated for BAPTA (Adler et al., 1991; Stern, 1992) or for 4,4′-F_2-BAPTA (Speksnijder et al., 1989). Data in Table 3 give pilot values from which a requirement of $[Ca^{2+}]_i^{act}$ of 1 μM or somewhat more can be derived. This is compatible (i) with our $[Ca^{2+}]$ imaging values, and (ii) with the threshold free Ca^{2+}-concentration causing trichocyst exocytosis after Ca^{2+} injection. None of these data can exclude the possibility, however, that a very locally higher $[Ca^{2+}]_i^{act}$ may occur, particularly since Ca^{2+} buffers have recently been shown to entail some uncertainties on their own (Borst and Sackmann, 1996; Neher, 1996).

From the volume of a *Paramecium* cell (0.7×10^{-10} l; Erxleben et al., 1997) and the data for Ca^{2+} influx and pool mobilisation (see above), a global $[Ca^{2+}]_i^{act}$ = 2 mM would result. This is ~10^4 times above global peak values observed with nd9-28°C or tl cells, respectively. Injection of 500 μM Ca^{2+} induced a global rise of free $[Ca^{2+}]_i$ to ~500 nM, indicating a Ca^{2+} binding ratio of ~100 for *Paramecium* cytoplasm, a value well comparable to the Ca^{2+}-buffer capacity of other systems (Neher, 1995). We assumed that ~99% of Ca^{2+} would be rapidly bound to cytosolic proteins (Neher and Augustine, 1992; Helmchen et al., 1996), ~99% of the remaining Ca^{2+} would have to be removed in another way (see Conclusions, below). Evidently after AED stimulation the different strains operate with different kinetics to re-establish $[Ca^{2+}]$ homeostasis, whereby the state of trichocyst docking sites might play a role.

Conclusions

Despite some uncertainties (which are not unique to our own work) we can derive from our analyses several important conclusions. (i) Trichocyst exocytosis is accompanied by a cortical $[Ca^{2+}]$ increase in the subsecond time range. (ii) This increase occurs also with mutants with defective or missing targets. (iii) As to the ensuing $[Ca^{2+}]$ increase in deeper cell regions we want to speculate along the following lines. The cell body serves as a sink for the tremendous excess of Ca^{2+}, from influx and store mobilisation, which is required for a successful exo-endocytosis cycle (Plattner et al., 1997a). This spillover accounts for dilution by diffusion and favours binding to endogenous buffers throughout the cell body. Sequestration into endoplasmic reticulum, occurring throughout the cell body and endowed with calreticulin-like protein (Plattner et al., 1997b), will also facilitate re-establishment of Ca^{2+} homeostasis, within >20 seconds, after AED stimulation.

We thank Dr J. Beisson (CNRS, Gif-sur-Yvette) for providing the nd9 mutant, Dr J. Hentschel for setting up CLSM technology, Mrs R. Schmidt, D. Schmid and W. Schweinbeck for the filter wheel design. This study was supported by DFG grant Pl78/12-2.

REFERENCES

Adler, E. M, Augustine, G. J., Duffy, S. N. and Charlton, M. P. (1991). Alien intracellular calcium chelators attenuate neurotransmitter release at the squid giant synapse. *J. Neurosci.* **11**, 1496-1507.

Augustine, G. J. and Neher, E. (1992). Calcium requirements for secretion in bovine chromaffin cells. *J. Physiol.* **450**, 247-271.

Bacskai, B. J., Wallen, P., Lev-Ram, V., Grillner, S. and Tsien, R. Y. (1995). Activity-related calcium dynamics in lamprey motoneurons as revealed by video-rate confocal microscopy. *Neuron* **14**, 19-28.

Beisson, J., Lefort-Tran, M., Pouphile, M., Rossignol, M. and Satir, B. (1976). Genetic analysis of membrane differentiation in *Paramecium*. Freeze-fracture study of the trichocyst cycle in wild-type and mutant strains. *J. Cell Biol.* **69**, 126-143.

Bootman, M. D. and Berridge, M. J. (1995). The elemental principles of calcium signaling. *Cell* **83**, 675-678.

Borst, J. G. G. and Sackmann, B. (1996). Calcium influx and transmitter release in a fast CNS synapse. *Nature* **383**, 431-434.

Burgoyne, R. D. and Morgan, A. (1993). Regulated exocytosis. *Biochem. J.* **293**, 305-316.

Cheek, T. R. and Barry, A. (1993). Stimulus-secretion coupling in excitable cells: A central role for calcium. *J. Exp. Biol.* **184**, 183-196.

Chow, R. H., Klingauf, J. and Neher, E. (1994). Time course of Ca^{2+} concentration triggering exocytosis in neuroendocrine cells. *Proc. Nat. Acad. Sci. USA* **91**, 12765-12769.

Clapham, D. E. (1995). Calcium signaling. *Cell* **80**, 259-268.

Eckert, R. and Brehm, P. (1979). Ionic mechanisms of excitation in Paramecium. *Annu. Rev. Biophys. Bioeng.* **8**, 353-383.

Eilers, J., Callewaert, G., Armstrong, C. and Konnerth, A. (1995). Calcium signaling in a narrow somatic submembrane shell during synaptic activity in cerebrellar Purkinje neurons. *Proc. Nat. Acad. Sci. USA* **92**, 10272-10276.

Erxleben, C. and Plattner, H. (1994). Ca^{2+} release from subplasmalemmal stores as a primary event during exocytosis in *Paramecium* cells. *J. Cell Biol.* **127**, 935-945.

Erxleben, C., Klauke, N., Flötenmeyer, M., Blanchard, M. P., Braun, C. and Plattner, H. (1997). Microdomain Ca^{2+} activation during exocytosis in *Paramecium* cells. Superposition of local subplasmalemmal calcium store activation by local Ca^{2+} influx. *J. Cell Biol.* **136**, 597-607.

Föhr, K. J., Warchol, W. and Gratzl, M. (1993). Calculation and control of free divalent cations in solutions used for membrane fusion studies. *Meth. Enzymol.* **221**, 149-157.

Grapengiesser, E. (1993). Cell photodamage, a potential hazard when measuring cytoplasmic Ca^{2+} with Fura-2. *Cell Struct. Funct.* **18**, 13-17.

Helmchen, F., Imoto, K. and Sackmann, B. (1996). Ca^{2+} buffering and action potential-evoked Ca^{2+} signaling in dendrites of pyramidal neurons. *Biophys. J.* **70**, 1069-1081.

Kerboeuf, D. and Cohen, J. (1990). A Ca^{2+} influx associated with exocytosis is specifically abolished in a *Paramecium* exocytotic mutant. *J. Cell Biol.* **111**, 2527-2535.

Kersken, H., Vilmart-Seuven, J., Momayezi, M. and Plattner, H. (1986). Filamentous actin in *Paramecium* cells: Mapping by phalloidin affinity labeling in vivo and in vitro. *J. Histochem. Cytochem.* **34**, 443-454.

Knoll, G., Braun, C. and Plattner, H. (1991). Quenched-flow analysis of exocytosis in *Paramecium* cells: Time course, changes in membrane structure and calcium requirements revealed after rapid mixing and rapid freezing of intact cells. *J. Cell. Biol.* **113**, 1295-1304.

Knoll, G., Kerboeuf, D. and Plattner, H. (1992). A rapid calcium influx during exocytosis in *Paramecium* cells is followed by a rise in cyclic GMP within 1s. *FEBS Lett.* **304**, 265-268.

Llinás, R., Sugimori, M. and Silver, R. B. (1995). The concept of calcium concentration microdomains in synaptic transmission. *Neuropharmacol.* **34**, 1443-1451.

Lumpert, C. J., Kersken, H. and Plattner, H. (1990). Cell surface complexes ('cortices') isolated from *Paramecium tetraurelia* cells as a model system for analysing exocytosis *in vitro* in conjunction with microinjection studies. *Biochem. J.* **269**, 639-645.

Machemer, H. (1989). Cellular behaviour modulated by ions: Electrophysiological implications. *J. Protozool.* **36**, 463-487.

Minta, A., Kao, J. P. Y. and Tsien, R. Y. (1989). Fluorescent indicators for cytosolic calcium based on rhodamine and fluorescein chromophores. *J. Biol. Chem.* **264**, 8171-8178.

Morgan, K. G. (1993). $Ca^{2+}{}_i$ versus $[Ca^{2+}]_i$. *Biophys. J.* **65**, 561-562.

Naitoh, Y. and Kaneko, H. (1972). Reactivated Triton-extracted models of *Paramecium*: Modification of ciliary movement by calcium ions. *Science* **176**, 523-524.

Nakaoka, Y., Tanaka, H. and Oosawa, F. (1984). Ca^{2+}-dependent regulation of beat frequency of cilia in *Paramecium*. *J. Cell Sci.* **65**, 223-231.

Neher, E. and Augustine, G. J. (1992). Calcium gradients and buffers in bovine chromaffin cells. *J. Physiol.* **450**, 273-301.

Neher, E. (1995). The use of Fura-2 for estimating Ca buffers and Ca fluxes. *Neuropharmacol.* **34**, 1423-1442.

Neher, E. (1996). Help from fast synapses. *Nature* **383**, 393-394.

Pethig, R., Kuhn, M., Payne, R., Adler, E., Chen, T. H. and Jaffe, L. F. (1989). On the dissociation constants of BAPTA-type calcium buffers. *Cell Calcium* **10**, 491-498.

Plattner, H., Matt, H., Kersken, H., Haacke, B. and Stürzl, R. (1984). Synchronous exocytosis in *Paramecium* cells. I. A novel approach. *Exp. Cell Res.* **151**, 6-13.

Plattner, H., Stürzl, R. and Matt, H. (1985). Synchronous exocytosis in *Paramecium* cells. IV. Polyamino compounds as potent trigger agents for repeatable trigger-redocking cycles. *Eur. J. Cell Biol.* **36**, 32-37.

Plattner, H., Lumpert, C. J., Knoll, G., Kissmehl, R., Höhne, B., Momayezi, M. and Glas-Albrecht, R. (1991). Stimulus-secretion coupling in *Paramecium* cells. *Eur. J. Cell Biol.* **55**, 3-16.

Plattner, H., Braun, C. and Hentschel, J. (1997a). Facilitation of membrane fusion during exocytosis and exocytosis-coupled endocytosis and acceleration of 'ghost' detachment in *Paramecium* by extracellular calcium. A quenched-flow/freeze-fracture analysis. *J. Membr. Biol.* (in press).

Plattner, H., Habermann, A., Kissmehl, R., Klauke, N., Majoul, I. and Söling, H. D. (1997b). Differential distribution of calcium-stores in *Paramecium* cells. Occurrence of a subplasmalemmal store with a calsequestrin-like protein. *Eur. J. Cell Biol.* **72**.

Pollack, S. (1974). Mutations affecting the trichocysts in *Paramecium aurelia*. I. Morphology and description of the mutants. *J. Protozool.* **21**, 352-362.

Regehr, W. G. and Atluri, P. P. (1995). Calcium transients in cellular granule cell presynaptic terminals. *Biophys. J.* **68**, 2156-2170.

Ross, W. N. (1993). Calcium on the level. *Biophys. J.* **64**, 1665-1666.

Speksnijder, J. E., Miller, A. L., Weisenseel, M. H., Chen, T. H. and Jaffe, L. F. (1989). Calcium buffer injections block fucoid egg development by facilitating calcium diffusion. *Proc. Nat. Acad. Sci. USA* **86**, 6607-6611.

Stelly, N., Mauger, J. P., Kéryer, G., Claret, M. and Adoutte, A. (1991). Cortical alveoli of *Paramecium*: A vast submembranous calcium storage compartment. *J. Cell Biol.* **113**, 103-112.

Stelly, N., Halpern, S., Nicolas, G., Fragu, P. and Adoutte, A. (1995). Direct visualization of a vast cortical calcium compartment in *Paramecium* by secondary ion mass spectrometry (SIMS) microscopy: possible involvement in exocytosis. *J. Cell Sci.* **108**, 1895-1909.

Stern, M. D. (1992). Buffering of calcium in the vicinity of a channel pore. *Cell Calcium* **13**, 183-192.

Tsien, R. Y. (1988). Fluorescence measurement and photochemical manipulation of cytosolic free calcium. *Trends Neurosci.* **11**, 419-424.

Tsien, R. W. and Tsien, R. Y. (1990). Calcium channels, stores and oscillations. *Annu. Rev. Cell Biol.* **6**, 715-760.

Zucker, R. S. (1993). Calcium and transmitter release at nerve terminals. *Biochem. Soc. Trans.* **21**, 395-401.

(Received 28 August 1996 - Accepted, in revised form, 14 February 1997)